Presented at the IEEE/ASME/IEE 5th International Conference on Mechatronics and Machine Vision in Practice, September 1998, Nanjing, China.

Design and Analysis of a Foundry Fabricated Surface-Micromachined Rotation Sensor

Winston Sun[1], Tin-Tak Tsang, and Wen J. Li
Department of Mechanical and Automation Engineering, The Chinese University of Hong Kong

John D. Mai, and Chih-Ming Ho
Department of Mechanical and Aerospace Engineering, University of California, Los Angeles

ABSTRACT

A novel MEMS surface-micromachined non-contact rotation sensor with total surface area under 4mm^2 is now under development. Various versions of the sensor have been designed and are currently under production using the MCNC MUMPS fabrication process. The direction of rotation and angular acceleration of rotating disks with different diameters will be measured using these sensors via wireless transmission. This paper presents the design and performance analysis of these foundry-fabricated sensors. The experimental setup and initial RF wireless transmitted signals using two different methods are also presented.

1. INTRODUCTION

Tachometers have been widely used to measure the angular speeds of rotating objects. In general, contact mechanical-based tachometers, although capable of giving measurements conveniently, are less accurate than AC or DC electromagnetic-based tachometers. Nevertheless, each type has its own advantages and disadvantages depending on the applications [1,2]. Optical tachometers are also available that give relatively accurate readings with wide rpm range [3,4]. However, Kwa et al. [5] pointed out that some optical sensors are quite sensitive to background light and contamination.

Recently, many new sensor devices based on different principles, including non-contact magnetic field (Watanabe et al. [6]), Faraday induction (Powell et al. [7]), and capacitive (Fabian et. al. [8]), have been built. These techniques, however, impose restrictions on the material properties or geometry of the rotational components to be measured, and they also limit the effective measurable rotation speed. In addition, all these sensors must be accompanied with a stationary reference, which is externally mounted to the systems' housing for proper operation. Imagine a mechanical transmission system or a gearbox assembly with lots of gears. If for diagnostic purpose the angular speed of each individual gear is to be measured, then traditional tachometers might not be a good solution.

We propose to build a MEMS rotation sensor that can be potentially integrated with wireless-transmission electrical circuitry. Since these micromachined sensors will be small, they can be directly embedded into the rotating objects such as gears or shafts, hence no sensor reference mounting is needed.

Many MEMS rotation sensors have been fabricated using piezoelectric, piezoresistive, or capacitive principles (e.g., Ref. 9,10, and11). However, the existing sensors are designed mainly for low angular speed and acceleration measurements. In addition, to the best of our knowledge, no sensors were built using a commercial foundry service and have wireless transmitted output.

This paper presents the design and analysis of polysilicon cantilever beam rotation sensors which can measure angular speeds between 1000 to 5000 rpm. These sensors are designed to have small size, low power consumption, low cost, wide dynamic range, and yet accurate. For demonstration, we have selected to use the MCNC MUMPS foundry to fabricate the mechanical elements that will then be interfaced with commercial wireless transmission chips. If the concept is proved to be successful, then these non-contact sensors can be batch fabricated and will become commercially viable.

2. SENSOR DESIGN

The conceptual design of the sensor is shown in Figure 1. L_{be} differs from L_{bm} in which the former length is measured from the edge of the platform to the connection pad, while the latter length is measured from that to the anchor position. Electrical resistance is computed in terms of L_{be}, and moment about the fixed end is represented by L_{bm}. Dimples support the mass platform and prevent it from sticking to the substrate when the entire system is at rest. The L-Edit® cross-section view is shown in Figure 2. As shown, the connection pad is anchored to the nitride layer. The oxide layer underneath the mass platform will be sacrificially released. Etches holes are needed to provide shorter release etch paths under large polysilicon features like the mass platform, which is supported only by two cantilever beams and therefore is free for deflection by centrifugal forces.

[1] Email: wsun@mae.cuhk.edu.hk. Rm. 232 HSH building, CUHK, NT, Hong Kong. (852) 2609-8469

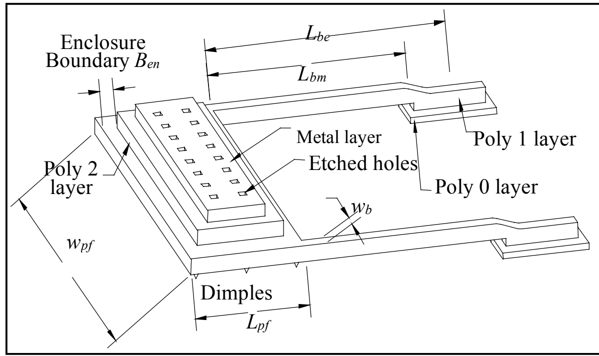

Figure 1. Conceptual drawing of the cantilever beam rotation sensor (not to scale).

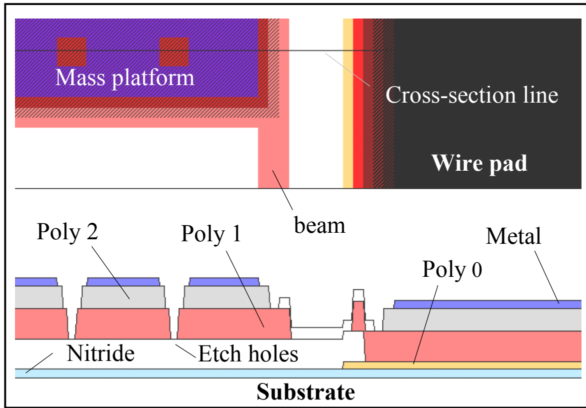

Figure 2. Cross-sectional view of the seismic mass and the cantilever beams. The view is generated by L-Edit®.

The seismic mass of this sensor is, unlike some accelerometers, supported by 2 instead of 1 cantilever beams for stability purposes. As seen in Figure 3, a set containing two identical sensors in opposite direction is oriented so that the axes of the cantilever beams are perpendicular to the axis of rotation. As will be discussed later, a set of 2 sensors is needed to measure the angular acceleration of the rotating element. If no linear motion along the rotation axis then lateral deflection of the beams, or transverse stress, can be neglected. Excluding the substrate, a stationary sensor is less than 5.1μm thick and weights about 15μg.

Figure 4 is a conceptual drawing of the test setup for measuring the rotation speed of a disk wirelessly using MCNC fabricated sensors. In our design the rotating disk is replaceable. Another sensor set with the same beam and platform dimensions is placed in the other side of the rotating disk as shown in Figure 4 and used as reference sensors. The seismic mass and cantilever beams of these sensors are anchored to the nitride layer such that no stress is induced on the beam by centrifugal forces. The power supply, which is just a 3V lithium watch battery, and the wireless data transmission chips are placed within a small package made by a CNC plastic injection machine which will be placed on the disks as illustrated in Figure 4. We have made Aluminum disks with center-to-sensors distance of 2cm, 3cm, 4cm, and 5cm. A 2cm disk is shown in Figure 5.

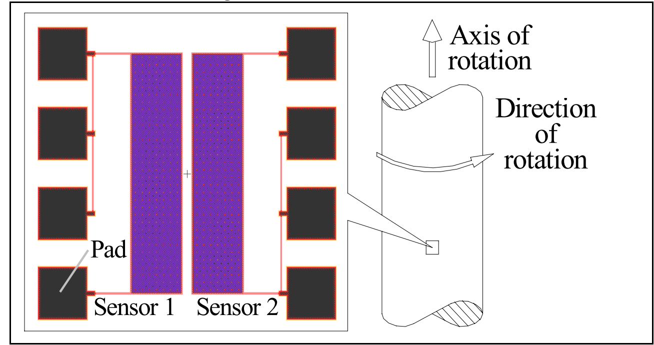

Figure 3. L-Edit® layout view of a set of sensors which can be embedded perpendicularly to the axis of rotation.

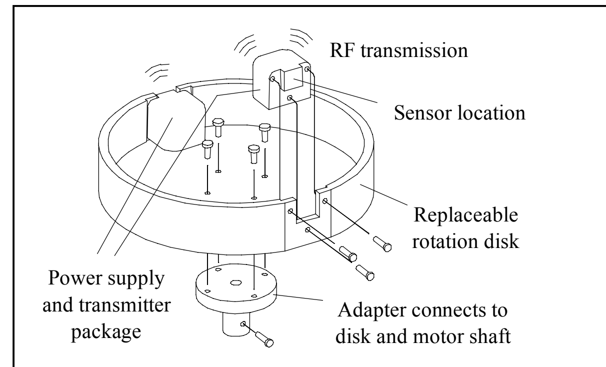

Figure 4. Conceptual drawing of the experimental rotating disk packaged with wireless rotation MEMS sensors.

Figure 5. A 2cm center-to-sensor disk.

Angular Velocity Measurement

The side view of a stationary sensor is illustrated in Figure 6. As shown, the initial moment arm from the centroid c to the fixed end F is a constant. When a centrifugal force is induced on the seismic mass by an angular velocity (ω) or acceleration (α), the length of this moment arm will change. From Figure 7 we can observe that the transverse load $P = m \cdot r \cdot \omega^2$ induced by rotation and the axial load $N = m \cdot r \cdot \alpha$ caused by angular acceleration (r is the distance from the axis of rotation to the seismic

mass) both act on the centroid c of the platform. The distance e_c is a constant depending on the number of polysilicon layers. It is measured from the centroid of the platform to the neutral axis of the beam. The maximum strain on the cantilever beams occurs at F, the fixed end of the beams. From Fan et al. [12] the maximum allowable strain of polysilicon is taken to be 1.7%. At $t > 0$ sec, the platform will be raised by a distance h_{cg} due to centrifugal force. Consequently the beams will be under stress and deformed in a curved shape. The beams will also undergo slight elongation or shortening depending on the combined effect of P and N. The moment arm measured from the fixed end to the centroid will also be shifted from initial distance to arm_{cg}.

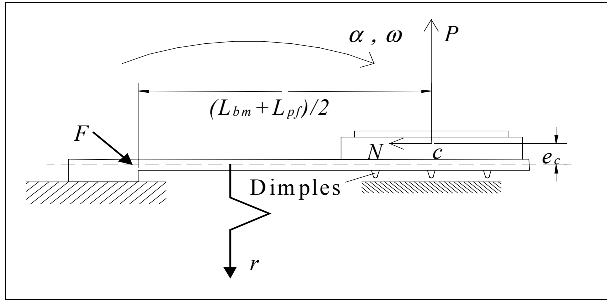

Figure 6. Sideview of the MCNC rotation sensor.

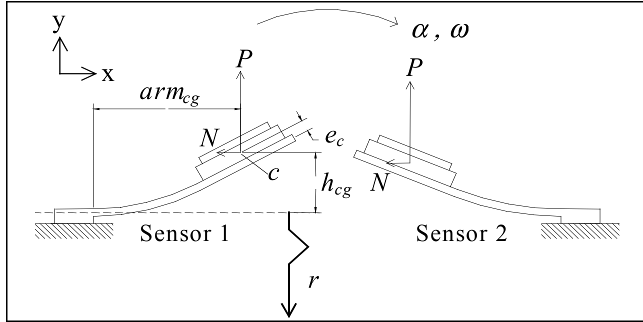

Figure 7. Deflection caused by transverse load P and axial load N.

The governing differential equation for the bending beam is shown in Equation 1. The moment and stress equations are shown in Equations 2 and 3, respectively.

$$EI\frac{d^2 y_i}{dx_i^2} + P \cdot x \pm N \cdot y - M_i = 0 \qquad (1)$$

$$M_i = P \cdot arm_{cg} \pm N \cdot h_{cg} \qquad (2)$$

$$\sigma_i = M_i \cdot (t_{bm}/2)/I_{bm} \quad N/A_{bm}\ , \qquad i = 1, 2 \qquad (3)$$

The index i denotes sensors 1 and 2 in Figure 7. In Equation 3 I_{bm} is the moment of inertia of the cross-section area about the neutral axis. $A_{bm} = t_{bm} \cdot (2 \cdot w_{bm})$ is the total cross-section area of the two beams. Equation 1 is obtained by summing the moments about any arbitrary point (x_i, y_i) along the beam i. Analytical solutions of Equation 1 can be readily obtained from symbolic mathematical packages (i.e., Mathematica) for a given set of values of r, ω and α. For transient calculations, the results of Equation 1 can be used to obtain arm_{cg} and h_{cg} at a given time, which can then be used in Equation 2 to obtain a more accurate solution. An example of the analytical solution to the bending of the cantilever beams is shown in Figure 8. In the figure, the thicker lines represent the seismic mass and the thinner lines represent the deflected beams. The centroid of the seismic mass are represented by the circles.

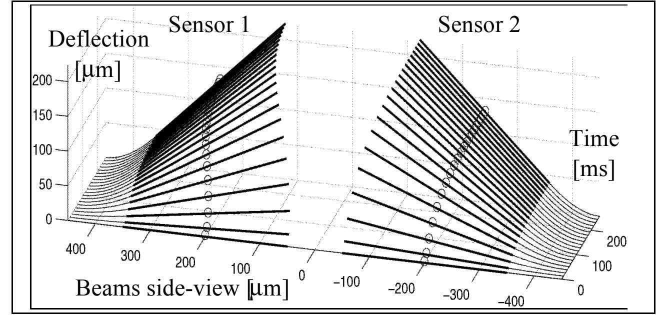

Figure 8. Theoretical results of the seismic mass response to centrifugal force over time.

The deflection or elongation of the beams causes a change of resistance of the polysilicon, which can be converted into a measurable change of voltage by connecting the sensors in a Wheatstone bridge configuration [13]. The change of resistance due to beam elongation can be expressed as a function of gauge factor G or in terms of the piezoresistance coefficient π_{44} [14]. This is shown in Equation 4,

$$\frac{\Delta R_i}{R} = \underbrace{\frac{G}{L_{bm}} \cdot \int_0^{L_{bm}} \frac{\sigma_i}{E} dx}_{C_{Gi}} = \underbrace{\frac{\pi_{44}}{2} \cdot (\sigma_{li} - \sigma_{ti})}_{C_{\pi i}} \qquad (4)$$

where R is the total resistance of the sensor and for polysilicon is typically about 10 Ω/□ [15]. π_{44} is taken to be 138.1×10^{-11} Pa^{-1}, a result published by Smith [16] in 1954 and verified by Beaty et al. [0] in 1992. σ_l is the longitudinal stress in Equation 1, and σ_t is the transverse stress which can be neglected at steady state conditions. A comparison of $\Delta R/R$ calculated using G and π_{44} for Sensor 1 is shown in Figure 9. As indicated, the predicted results are very similar. The transient startup characteristics from a commercial motor was used to obtain the time-dependent angular velocity information in getting the solution in Figure 9.

Five different versions of the sensor were designed and relevant design parameters are shown in Table 1.

Version	w_b	L_{bm}	w_{pf}	L_{pf}	Beam constant	Stationary resistance
	[µm]				[N/m]	[Ω]
1	6	100	690	1200	0.36	350
2	12	100	690	1200	0.72	170
3	12	100	1290	300	2.22	210
4	12	100	690	300	2.22	190
5	12	200	1290	300	0.42	390

Table 1. Dimensions of different versions of the sensors.

The dimensions of the platform and the cantilever beams have direct effect on the overall resistance. From Table 1 we can see that versions 3 and 4 were designed to be less sensitive to obtain a wider dynamic range.

The theoretical change of resistance as a function of rotational speed of a sensor is shown in Figure 10.

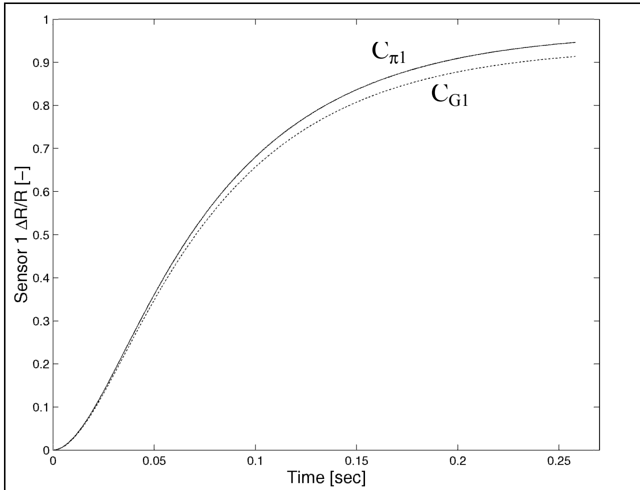

Figure 9. Theoretical results of ΔR/R as a function of time during the startup phase of a commercial motor. The results are computed using the gauge factor and the piezoresistive coefficient of polysilicon.

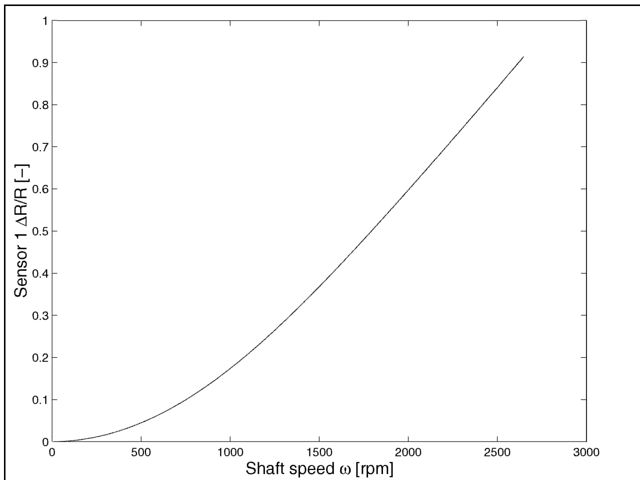

Figure 10. Theoretical results of ΔR/R as a function of ω.

Direction of Angular Acceleration Measurement

When a steady state rotational speed is achieved, axial load N tends to zero. The two sensors will have the same deflection and change of resistance. However, when the angular acceleration α is >> 0, such as during motor startup or under sudden change of speed, the transient response of Sensor 1 and Sensor 2 will be different due to the contribution from N (see Figure 7). Hence, by monitoring the transient response of the sensors, the direction of acceleration and be determined. The difference in $\Delta R/R$ for sensors 1 and 2 during the startup phase of a commercial motor is shown in Figure 11.

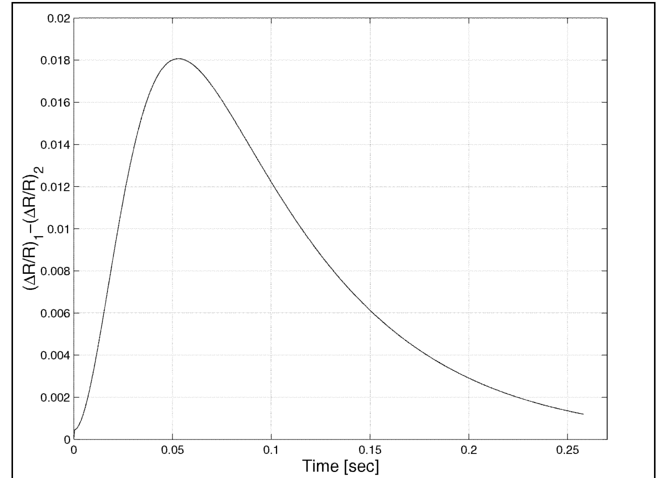

Figure 11. Theoretical output difference between a set of sensors which can be used to determine the direction of rotation.

3. WIRELESS TRANSMISSION

Commercial wireless transmitters and receivers which can be eventually interfaced with the MEMS sensors were evaluated for signal transmission. Two different configurations were evaluated. The first configuration, as shown in Figure 12, maps the analog voltage output from the sensor into digital data before RF transmission of the data by the transmitter. The volume of the entire transmitter circuitry, including the sensor, battery, and IC chip packaged ADC, clock, and RF transmitter is currently about 1cmx3cmx3cm. When the ADC, clock, and RF transmitter die are used instead of the IC packaged chips the entire transmitter circuitry should be significantly smaller.

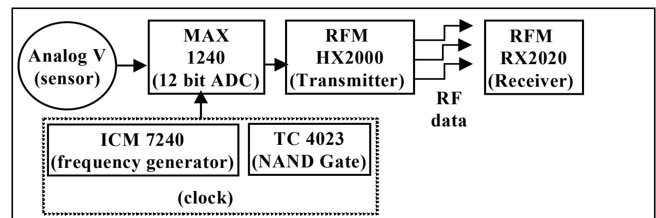

Figure 12. Block diagram for digital transmission of sensor data.

Examples of RF voltage transmission are shown in Figures 13 and 14. In Figure 13 an output voltage of 0.44 V is transmitted; in Figure 14 an output voltage of 1.9 V is transmitted. The 12-bit data from the receiver can then be deciphered to obtained source voltage output.

A second type of transmission scheme, which maps the voltage from a sensor into frequency before the RF transmission, is shown in Figure 15. The overall volume of the IC packaged chips for this scheme is

only 1/3 the size of the previous method but a frequency counter must be used at the receiver end to decipher the original voltage information. Sample of the frequency output versus the voltage input from the AD654 is shown in Figure 16. A linear relationship can be obtained as indicated. Although both scheme will give approximate the same overall volume when the components are interfaced in die form, they need to be evaluated for maximum output sensitivity of the sensor system.

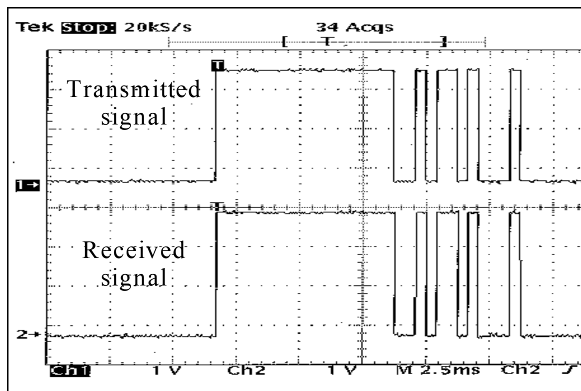

Figure 13. Signals transmitted by the RFM HX2000 and received by the RFM RX2020 from a DC voltage of 0.44V source.

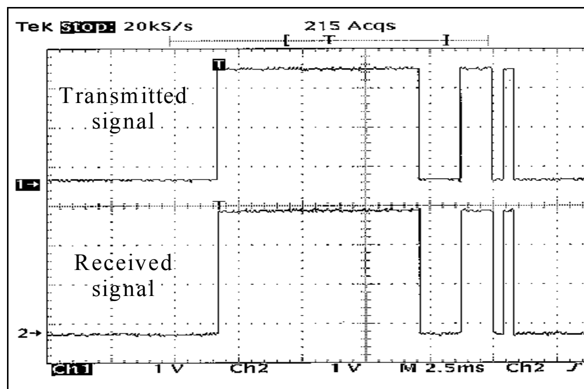

Figure 14. In this case, a source voltage of 1.9 V is transmitted.

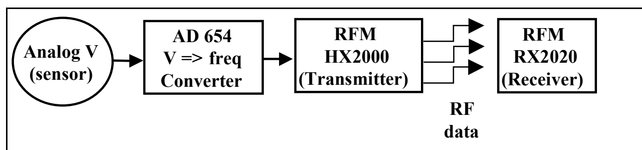

Figure 15. Block diagram for digital transmission of sensor data where the sensor data is mapped to a frequency domain before transmission.

4. CONCLUSION

The design of a novel surface-micromachined rotation sensor is presented. It is designed to detect the angular velocity of a rotating element by measuring the resistance change due to stress induced by centrifugal force on the seismic mass based on the piezoresistive effect. Likewise, the angular acceleration and direction of rotation can also be estimated. The sensor can be directly embedded onto the rotating element of a mechanical system. Two wireless transmission schemes for the rotation sensors were evaluated and the preliminary results were presented. Experiments on the mechanical sensor component will be to verify the simulation results as soon as MUMPS25 is complete. Testing and calibration procedures will also be accomplished in order to ensure the sensor gives accurate and reliable data.

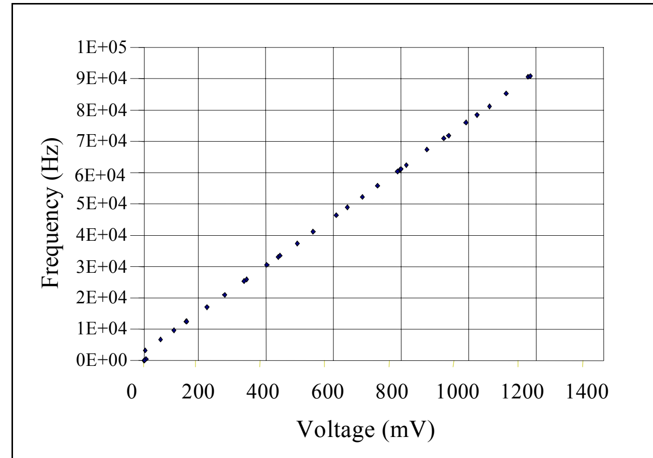

Figure 16. Frequency output versus voltage of the AD 654 voltage-to-frequency converter.

REFERENCES

1. J. A. Haslam, et al., Engineering instrumentation and control, 1993, pp. 133.
2. C. L. Nachtigal, Instrumentation and control – Fundamentals and Applications, 1990, pp. 370.
3. http://catalogue.pwallen.co.uk
4. R. C. Spooncer, et al., “An optical tachometer with optical fibre links”, IEE Colloquium on IREM, 1991.
5. T. A. Kwa, et al., “An integrated high-resolution optical angular displacement sensor” IEEE Transducers '91, pp. 368-371.
6. K. Watanabe, et al., “Non-contact revolution measurement by the magnetic field intensity from axes”, IEEE IMTC '94, **2**, pp. 605-608.
7. A. Powell, et al., “Optimisation of magnetic speed sensors”, IEEE Trans. on Mag. '96, **32**, pp. 4977-9.
8. T. Fabian, et al., “A robust capacitive angular speed sensor”, IEEE IMTC '97, **2**, pp. 1267-1272.
9. J. Soderkvist, “Piezoelectric beams and angular rate sensors”, IEEE Proc. on the 44th Annual Symposium On Frequency Control, 1990.
10. A. M. Madni, et al., “A microelectromechanical quartz rotational rate sensor for inertial applications”, IEEE Aeros. App. Conf., 1996, **2**, pp. 315-332.
11. R. Voss, et al., “Silicon angular rate sensor for automotive applications with piezoelectric drive and piezoresistive read-out”, IEEE TRANSDUCERS '97, **2**, pp. 879-882.
12. L. S. Fan, et al., IEEE Trans. on Electron Devices, 1988, **35**. pp. 724-730.

13. T. G. Beckwith, et al., Mechanical measurements, 3rd edition, 1982.
14. B. Kloeck, "Piezoresistive sensors", Sensors – A comprehensive survey, 1994, **7**, pp. 158-163.
15. D. A. Koester, et al., SmartMUMPS Design Handbook including MUMPs introduction and Design Rules Rev. 4.0, MEMS Technology Applications Center, March 1996.
16. C. S. Smith, Phys. Rev. 94, 1954, pp. 42-49.

R. E. Beaty, et al., "Evaluation of Piezoresistive coefficient variation in silicon stress sensors using a four-point bending test fixture", IEEE Trans. on CHMT '92, **15**, pp. 904-914.